Journal of Magnetic Resonance 209 (2011) 207–219

Contents lists available at ScienceDirect

Journal of Magnetic Resonance

journal homepage: www.elsevier.com/locate/jmr

Radio frequency assisted homonuclear recoupling – A Floquet description of homonuclear recoupling via surrounding heteronuclei in fully protonated to fully deuterated systems

Michal Leskes [a,1], Ümit Akbey [b], Hartmut Oschkinat [b], Barth-Jan van Rossum [b], Shimon Vega [a,*]

[a] Department of Chemical Physics, Weizmann Institute of Science, Rehovot 76100, Israel
[b] Leibniz-Institut für Molekulare Pharmakologie (FMP), Robert-Rössle-Str. 10., 13125 Berlin, Germany

ARTICLE INFO

Article history:
Received 28 November 2010
Revised 9 January 2011
Available online 18 January 2011

Keywords:
Solid state NMR
MAS
^{13}C–^{13}C recoupling
DARR
RAD
DONER
Perdeuterated proteins
Floquet theory

ABSTRACT

We present a Floquet theory approach for the analysis of homonuclear recoupling assisted by radio frequency (RF) irradiation of surrounding heteronuclear spins. This description covers a broad range of systems from fully protonated to deuterated proteins, focusing in detail on recoupling via protons and deuterons separately as well as simultaneously by the double nucleus enhanced recoupling (DONER) scheme. The theoretical description, supported by numerical simulations and compared to experimental results from a partially deuterated model compound, indicates that in perdeuterated systems setting the RF amplitude equal to the magic angle spinning (MAS) frequency is not necessarily optimal for recoupling via ^{1}H and/or ^{2}H nuclei and modified recoupling conditions are identified.

1. Introduction

Homonuclear recoupling techniques are a basic tool in the study of protein structure with solid state NMR (ssNMR). Most commonly these studies are based on isotope enrichment of either ^{15}N or ^{13}C nuclei or both [1,2]. The relatively weak homonuclear dipolar interactions between these low gamma nuclei are easily averaged out by magic angle spinning (MAS) to produce high resolution spectra. These line broadening interactions are, however, essential for forming correlations between spins, which can then be analyzed for spectral assignment and structure determination.

Several approaches exist for the reintroduction of homonuclear couplings under MAS conditions. One type of recoupling experiments is based solely on the interacting spin pairs. Such is the rotational resonance (R^2) experiment in which the MAS frequency is set equal to the isotropic chemical shift difference between the spins [3,4]. The dipolar interaction can also be actively recoupled by radio frequency (RF) pulses at the frequency of the interacting nuclei. Numerous sequences have been developed towards this goal including dipolar recoupling at the magic angle (DRAMA) [5,6], radio-frequency driven recoupling (RFDR) [7], double quantum (DQ) homonuclear rotary resonance (HORROR) [8], symmetry based schemes such as POST-C7 [9] and SPC5 [10] and mixing by stochastic recoupling [11]. These and many additional schemes are reviewed in ref. [12].

Another approach to homonuclear recoupling is assisted by the surrounding protons which are highly abundant and form a strong network of couplings. In the passive approach, called proton driven spin diffusion (PDSD) [13], no RF is applied and the strong heteronuclear and homonuclear proton couplings mediate the formation of matching conditions between the low-gamma pairs and efficient recoupling of their homonuclear interaction. Alternatively, the surrounding protons can be used actively by irradiating them with RF pulses with an amplitude set equal to the MAS frequency, the so called rotary resonance recoupling (R^3) condition [14]. When the proton RF is turned on during the mixing time of a two dimensional (2D) experiment it assists in forming correlations between homonuclear pairs coupled to these protons. This type of 2D experiment is called dipolar assisted rotational resonance [15,16] (DARR) or RF assisted diffusion [17] (RAD). It was also shown that off-R^3 conditions can also lead to efficient recoupling via a modified mechanism named resonance interference recoupling (RIR) [16] or mixed rotational and rotary resonance (MIRROR) which is suitable for fast MAS [18]. The later can also be made less sensitive to RF inhomogeneity by phase or amplitude modulation. Phase alternation is also used in a scheme called PARIS for similar reasons [19]. Several new sequences were recently introduced which com-

* Corresponding author. Fax: +972 8 934 4123.
E-mail address: shimon.vega@weizmann.ac.il (S. Vega).
[1] Present address: Chemistry Department, University of Cambridge, Lensfield Rd, Cambridge CB2 1EW, United Kingdom.

1090-7807/$ - see front matter © 2011 Elsevier Inc. All rights reserved.
doi:10.1016/j.jmr.2011.01.015

bine the two approaches: irradiating both the homonuclear pairs and their surrounding heteronuclei. Among these are the proton assisted recoupling [20] (PAR) and the resonant second order transfer experiment [21] (RESORT).

In all these recoupling methods the strong heteronuclear couplings increase the efficiency of the recoupling process. On the other hand, the complicated network of homonuclear couplings between the protons prevents them from being more accessible themselves for structural studies, as they are in the study of soluble proteins. Furthermore, outside of the mixing period they are often a nuisance, causing line broadening when ^{13}C or ^{15}N are detected and require the application of either high power heteronuclear decoupling or very fast MAS frequencies. To overcome these difficulties the proton network is diluted by fully deuterating the protein followed by re-protonation of all or part of the exchangeable sites. This approach has lead to the introduction of many solution like experiments to proton based ssNMR as well as ^{13}C detection with only low power decoupling required [22–25]. In perdeuterated systems, however, common proton assisted recoupling techniques are not necessarily the most efficient. This has been recently demonstrated by Akbey et al. with the introduction of an efficient approach for homonuclear recoupling by double nucleus enhanced recoupling (DONER) [26]. In the DONER experiment carbon pairs are recoupled by the application of RF irradiation on both highly abundant deuterons and sparse protons. The superiority of the DONER scheme was demonstrated by the formation of new cross-peaks in ^{13}C homonuclear correlation experiments which were absent in the regular RAD/DARR schemes. Interestingly, the RAD experiment was originally demonstrated on partially deuterated systems where it was shown that deuteration helped in forming mostly long range carbon–carbon correlations between the carbons which were still coupled to protons [17]. An extensive study comparing the efficiency of several commonly used homonuclear recoupling schemes in perdeuterated proteins has been recently published [27].

The DONER experiment presents several methodological aspects which require consideration: What is the recoupling mechanism using RF irradiation of low abundance, weakly coupled, protons? How does the RF irradiation affect quadrupole nuclei which are only weakly coupled to the carbons? And finally, how do these two processes operate simultaneously? In order to investigate these issues we employ Floquet theory which allows us to derive a single framework describing all the various recoupling mechanisms and conditions. The DARR experiment itself has been previously studied using average Hamiltonian theory (AHT) in fully protonated systems where the heteronuclear couplings are strong [16]. Floquet theory was recently used in the description of the MIRROR scheme [18] and its relation to the DARR experiment has been discussed [28].

Here we present a step by step derivation of the Floquet Hamiltonian for the DONER experiment. Each of the recoupling processes, via protons and via deuterons, is discussed separately. A wide range of RF amplitudes is considered (not only at the R^3 condition), in order to get a broader understanding of the recoupling mechanisms. These are referred to as generalized RAD/DARR recoupling as they take into account the R^3 conditions. Several approaches are described for getting insight into systems with varying strength of heteronuclear couplings, ranging from fully protonated compounds with strong couplings, to dilute proton networks. Next the recoupling Hamiltonian for a deuterated system is considered where the most significant interaction is the quadrupole coupling which dominates the recoupling mechanism. Finally the two processes are combined and their mutual effect is discussed. The theoretical description is supported by numerical simulations and compared to experimental results from partly deuterated compounds.

2. Theory

2.1. RF assisted recoupling through surrounding spin 1/2 nuclei

2.1.1. The Floquet Hamiltonian

In order to appreciate the effect of homonuclear recoupling via RF irradiation on neighboring spin 1/2 heteronuclei, let us consider a system of two coupled ^{13}C nuclei additionally coupled to a single ^{1}H nucleus. We will later extend this description to include several protons and account for the effect of the homonuclear couplings between them. For the three spins system, the rotating frame Hamiltonian is given by

$$\mathscr{H}(t) = \mathscr{H}^{CS} + \mathscr{H}^{CC}(t) + \mathscr{H}^{HC}(t) + \mathscr{H}^{RF} \tag{1}$$

$$\mathscr{H}^{CS} = \omega_a C_{z,a} + \omega_b C_{z,b} \tag{2}$$

$$\mathscr{H}^{CC}(t) = \sum_{n=\pm1,\pm2} \omega_{ab} G^{CC}_{n,ab} \left(2C_{z,a}C_{z,b} - \frac{1}{2}\left(C_{+,a}C_{-,b} + C_{-,a}C_{+,b}\right)\right) e^{in\omega_r t} \tag{3}$$

$$\mathscr{H}^{HC}(t) = \sum_{n=\pm1,\pm2} \left\{ \omega_{aj} G^{HC}_{n,aj} H_{z,j} C_{z,a} + \omega_{bj} G^{HC}_{n,jb} H_{z,j} C_{z,b} \right\} e^{in\omega_r t} \tag{4}$$

$$\mathscr{H}^{RF} = \omega_1 H_x \tag{5}$$

where H_q and C_q (with $q = x,y,z$) are the linear spin angular momentum operators of the proton and carbon nuclei respectively, ω_a and ω_b are the isotropic chemical shifts of the carbon spins (the chemical shift anisotropy will be considered later) and the dipolar interactions are given by ω_{ab}, ω_{aj} and ω_{bj} for the homonuclear and heteronuclear pairs respectively. The magnitude of these dipolar interactions is given by $\omega_{ij} = \mu_0 \gamma_i \gamma_j \hbar / 4\pi r_{ij}^3$ where r_{ij} is the distance between the interacting nuclei i and j. The orientation dependence of the dipolar interactions is given by the $G^{CC}_{n,ab}$, $G^{HC}_{n,aj}$ and $G^{HC}_{n,bj}$ coefficients [29]. The RF irradiation is applied on resonance with an amplitude given by ω_1.

At this point it is often common to transform the rotating frame Hamiltonian to the RF interaction frame where it becomes modulated by two frequencies, that of the MAS, ω_r, and the RF amplitude, ω_1. However, since we would later consider the same Hamiltonian in the case of spin 1 (where the quadrupole coupling is the most dominant interaction and it is not justified to perform a transformation to the RF interaction frame), we will directly transform this Hamiltonian to its single mode Floquet representation (for details on this transformation see Ref. [30]). This is given by

$$\mathscr{H}_F = (\mathscr{H}^{CS}_0 + \mathscr{H}^{RF}_0)F_0 + \sum_n \left(\mathscr{H}^{CC}_n + \mathscr{H}^{HC}_n\right)F_n + \omega_r N \tag{6}$$

$$\mathscr{H}^{CS}_0 = \Sigma^{cs} C^{1-4}_z + \Delta^{cs} C^{2-3}_z \tag{7}$$

$$\mathscr{H}^{RF}_0 = \omega_1 H_z \tag{8}$$

$$\mathscr{H}^{CC}_n = \omega^{CC}_{n,ab}(C^{1-2}_z - C^{3-4}_z - C^{2-3}_x) \tag{9}$$

$$\mathscr{H}^{HC}_n = \Sigma^{HC}_{n,j} H_{x,j} C^{1-4}_z + \Delta^{HC}_{n,j} H_{x,j} C^{2-3}_z \tag{10}$$

Here we have used fictitious spin 1/2 operators to describe the carbon interactions [31]. With this representation the Floquet Hamiltonian is spanned by a basis set composed of a cross product between the Hilbert and Fourier states, given by $|\alpha\alpha,\nu,\pi> \equiv |1,\nu,\pi>$, $|\alpha\beta,\nu,\pi> \equiv |2,\nu,\pi>$, $|\beta\alpha,\nu,\pi> \equiv |3,\nu,\pi>$ and $|\beta\beta,\nu,\pi> \equiv |4,\nu,\pi>$ where ν represent the Fourier state and π stands for the proton states (this order of states is used for clarity). The interaction coefficients are given by $\Sigma^{cs} = \omega_a + \omega_b, \Delta^{cs} = \omega_a - \omega_b, \omega^{CC}_{n,ab} = \omega_{ab} G^{CC}_{n,ab}$, $\Sigma^{HC}_{n,j} = \omega_{aj} G^{HC}_{n,aj} + \omega_{bj} G^{HC}_{n,bj}$ and $\Delta^{HC}_{n,j} = \omega_{aj} G^{HC}_{n,aj} - \omega_{bj} G^{HC}_{n,bj}$. In addition we have tilted the proton interactions such that the RF is along the z direction.

2.1.2. Recoupling conditions

In this time independent Hamiltonian the CC interaction is off diagonal, connecting diagonal elements which are separated by the chemical shift difference and the MAS frequency. Examining

the form of the carbon interactions it can be expected that any recoupling process will involve only the |2> – |3> subspace of the carbon states (since for all the other combinations of states the interactions commute). The *CC* terms that can lead to recoupling connect the states $|2,v,\pi>$ and $|3,v+n,\pi>$, which are separated by $\Delta^{cs}+n\omega_r$. Since in most systems $\omega^{CC}_{n,ab}$ is fairly small (of the order of 1 – 2 kHz) it is negligible relative to this diagonal elements difference. In order for the *CC* interaction to become significant one should find a way to eliminate this difference. One possibility is to set the MAS frequency equal to the chemical shift difference, as is done in the R^2 experiment [3]. Another recoupling condition is used in the RAD [17] and DARR [15] recoupling experiments by exploiting the rotary resonance recoupling (R^3) [14], where the *CH* couplings become significant. To appreciate their effect let us consider the schematic representation of the Floquet Hamiltonian for the|2> – |3> subspace, plotted in Fig. 1. Examining the form of this Hamiltonian it is clear that the only elements which differ between the two diagonal blocks (|2> – |2> and |3> – |3>) and which can compensate for the chemical shift difference belong to the heteronuclear interaction. However, since they are off diagonal we first have to diagonalize the diagonal blocks and then consider their effect on the *CC* recoupling process. We can represent the |2> – |3> subspace Floquet Hamiltonians spanned by $|2,v,\pi>,|3,v,\pi>$ with $v=-\infty,\ldots,\infty$ as

$$\mathscr{H}_F^{2-3}=\sum_n\left\{\begin{pmatrix}\mathscr{H}_F^2 & 0\\ 0 & \mathscr{H}_F^3\end{pmatrix}+\begin{pmatrix}\frac{\Delta^{cs}}{2}\mathbf{I}F_0 & -\frac{\omega^{CC}_{n,ab}}{2}\mathbf{I}F_n\\ -\frac{\omega^{CC}_{n,ab}}{2}\mathbf{I}F_n & -\frac{\Delta^{cs}}{2}\mathbf{I}F_0\end{pmatrix}\right\} \tag{11}$$

$$\mathscr{H}_F^2=\omega_1H_zF_0+\frac{\Delta^{HC}_{n,j}}{2}H_{x,j}F_n+\omega_rN \tag{12}$$

$$\mathscr{H}_F^3=\omega_1H_zF_0-\frac{\Delta^{HC}_{n,j}}{2}H_{x,j}F_n+\omega_rN \tag{13}$$

where **I** is a unit matrix with dimensions given by the size of the proton spin system. In this representation $\mathscr{H}_F^2$ and $\mathscr{H}_F^3$ are spanned by the $|v,\pi>$ states and the contribution of the $\left(C_z^{1-2}-C_z^{3-4}\right)$ part in $\mathscr{H}_n^{CC}$ to the |2> – |3> subspace is neglected as it will not affect the following derivations.

In order to diagonalize $\mathscr{H}_F^2$ and $\mathscr{H}_F^3$ we can either apply a van Vleck transformation [32] for block diagonalization or perform a local exact diagonalization depending on the relative magnitude of the heteronuclear dipolar interactions ($|\Delta^{HC}_{n',j}|$) and the diagonal matrix elements they connect ($|\omega_1-n'\omega_r|$). In general, we can distinguish three possible routes to obtain the (approximated) diagonalized Hamiltonians Λ_F^2 and Λ_F^3:

(a) $|\Delta^{HC}_{n',j}|\ll|\omega_1-n'\omega_r|$: Away from a degeneracy in the Hamiltonians and when their off diagonal elements are small, the van Vleck transformations can be applied to obtain Λ_F^2 and Λ_F^3.

(b-i) $|\Delta^{HC}_{n',j}|<|\omega_1-n'\omega_r|$: In the vicinity of a degeneracy, as in the R^3 scheme when $\omega_1\simeq n'\omega_r$ (for a certain n' value) we must compare the off diagonal heteronuclear couplings matrix elements with the difference between the diagonal elements they connect, i.e. $(\omega_1-n'\omega_r)$. As long as these off diagonal elements are much smaller than $|\omega_1-n'\omega_r|$, the degeneracy has a very local and well defined position (in terms of the experimental parameters), so the van Vleck transformation is still justified and the recoupled off diagonal elements can be easily identified.

(b-ii) $|\Delta^{HC}_{n,j}|\geqslant|\omega_1-n'\omega_r|$ and $|\Delta^{HC}_{n,j}|<\omega_1,n\omega_r$: When the off diagonal elements are of the order of or larger than $(\omega_1-n'\omega_r)$, but not significantly larger than ω_1 and $n\omega_r$ themselves, we have to perform an exact diagonalization even when the degeneracy is not exactly met. In this case we can still ignore other off diagonal elements which do not connect nearly degenerate states.

(c) $|\Delta^{HC}_{n,j}|\gg\omega_1,n\omega_r$: Finally, when the off diagonal interactions are much larger than both ω_1 and $n\omega_r$ we have to perform an exact diagonalization taking into account all off diagonal elements (for all n values).

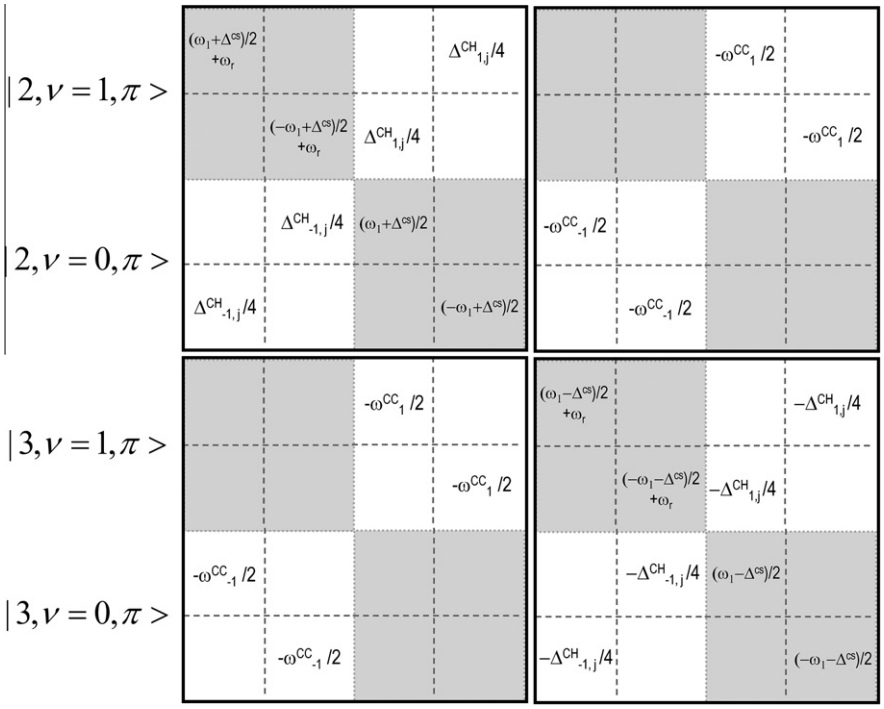

Fig. 1. A schematic representation of the |2 > – |3> subspace Hamiltonian describing a system of two carbons coupled to a single proton. For simplicity only the $v=1$, 0 Fourier states are shown. Carbon states are separated by black solid lines, diagonal Floquet blocks are in gray and off diagonal in white. The proton states are separated by dashed lines.

In the case of a carbon pair coupled directly to protons the *HC* interactions are relatively large and an exact diagonalization is necessary, following route (b-ii), of the relevant off diagonal terms. The diagonalization can be performed by diagonalizing sets of 2×2 matrices as has been discussed in detail in Ref. [30] and results in the following Hamiltonians

$$\Lambda_F^2 = \Lambda_F^3 = -\omega_{eff} H_{z,j} F_0 + \omega_r N \tag{14}$$

$$\omega_{eff} = \sqrt{|\frac{\Delta_{n',j}^{HC}}{2}|^2 + (\omega_1 - n'\omega_r)^2} - n\omega_r \tag{15}$$

For obtaining this effective Floquet Hamiltonian we have assumed that only the *CH* elements, which connect almost degenerate diagonal elements, are relevant, and that all other heteronuclear interaction terms can be neglected. Practically this means that these Hamiltonians, Λ_F^2 and Λ_F^3, are valid either in the vicinity of $\omega_1 = \omega_r$ (the $n' = 1$ R^3 condition), or of $\omega_1 = 2\omega_r$ (the $n' = 2$ R^3 condition). Away from these recoupling conditions (i.e. away from the R^3) we can use the van Vleck transformation (following route (a)).

After the diagonalization we observe that the two Hamiltonians are diagonal and equal, $\Lambda_F^2 = \Lambda_F^3$, thus it is not obvious that they compensate for the chemical shift difference between states |2> and |3>. This can be appreciated, however, when we consider the diagonalization matrices D_F^2 and D_F^3. Applying these matrices on $\mathscr{H}_F^{2-3}$ in Eq. (11) results in the following transformed off diagonal block Hamiltonian:

$$\widetilde{\mathscr{H}}_F^{2-3} = \left(D_F^{2-3}\right)^{-1} \mathscr{H}_F^{2-3} (D_F^{2-3}) \tag{16}$$

$$= \sum_n \begin{pmatrix} \Lambda_F^2 + \frac{\Delta^{cs}}{2}\mathbf{I}F_0 & -\frac{\omega_{n,ab}^{CC}}{2}\left(D_F^2\right)^{-1}(D_F^3)F_n \\ -\frac{\omega_{n,ab}^{CC}}{2}\left(D_F^3\right)^{-1}(D_F^2)F_n & \Lambda_F^3 - \frac{\Delta^{cs}}{2}\mathbf{I}F_0 \end{pmatrix} \tag{17}$$

with

$$D_F^{2-3} = \begin{pmatrix} D_F^2 & 0 \\ 0 & D_F^3 \end{pmatrix}. \tag{18}$$

In $\widetilde{\mathscr{H}}_F^{2-3}$ the *CC* interaction is still off diagonal, however, it does not necessarily connect the same proton states as in $\mathscr{H}_F^{2-3}$. The transformation (and change of basis set) when applied to the *CC* interaction results in elements connecting the same diagonal proton states as well as different proton states $|2, v, \pi>$ and $|3, v+n, \pi'>$ with $\pi \neq \pi'$. Since only the later can become degenerate, recoupling of the *CC* interaction via a generalized condition can occur when

$$\sqrt{\left|\frac{\Delta_{n',j}^{HC}}{2}\right|^2 + (\omega_1 - n'\omega_r)^2} + n\omega_r = \Delta^{cs} \tag{19}$$

with $|n| = 0, 1, 2, 3, 4$. For $\omega_1 = n'\omega_r$ this is the same condition described by Takegoshi et al. as DARR [16].

The extent of the part of the *CC* interaction which contributes to the recoupling depends on the diagonalization matrices. These can be evaluated and have the form:

$$D_F^2 = \cos\varphi_x \cos\varphi_z \mathbf{I}F_0 - 2i\cos\varphi_x \sin\varphi_z H_z F_0 - i\sin\varphi_x (e^{-i\varphi_z} H_+ F_{-n'} + e^{i\varphi_z} H_- F_{n'}) \tag{20}$$

$$D_F^3 = -\cos\varphi_x \cos\varphi_z \mathbf{I}F_0 - 2i\cos\varphi_x \sin\varphi_z H_z F_0 + i\sin\varphi_x (e^{-i\varphi_z} H_+ F_{-n'} + e^{i\varphi_z} H_- F_{n'}), \tag{21}$$

where

$$\tan 2\varphi_z = -1/\tan(\varphi_{n'}) \tag{22}$$

$$\tan 2\varphi_x = \frac{|\Delta_{n',j}^{CH}| \sin(\varphi_{n'})}{2(\omega_1 - n'\omega_r)} \tag{23}$$

for $\omega_1 \neq n'\omega_r$ and $2\varphi_x = \pi/2$ for $\omega_1 = n'\omega_r$. The phase factor $\varphi_{n'}$ is given by $\Delta_{n',j}^{CH} = |\Delta_{n',j}^{CH}| e^{i\varphi_{n'}}$ (and is related to the geometric coefficients of the heteronuclear dipolar couplings). Thus the magnitude of the elements of the *CC* interaction connecting the degenerate states, after the diagonalization, depends on the relative magnitude of the *CH* interaction and the deviation from the exact R^3 condition with significant recoupling when $\omega_1 = n'\omega_r$ is approached.

To demonstrate this dependence we consider a system of two carbons coupled to a single proton. Simulations of this system were performed using SPINEVOLUTION program [33] by applying on resonance RF irradiation on the proton for a fixed duration of $\tau_{mix} = 15$ ms. The detected signal is then calculated, by setting both the starting density matrix and the detection operator equal to C_z^{2-3}, and used to evaluate the extent of recoupling. Maximal recoupling is achieved when $\langle C_z^{2-3}\rangle(\tau_{mix}) = -\langle C_z^{2-3}\rangle(t=0) = -1$. Here, as well as in the following sections, we do not consider the rates of the signal build-up (for $\tau_{mix} = 15$ ms the signal reaches a plateau at a value which depends on the powder average).

The simulated powder averaged signal is plotted in Fig. 2a–c as a function of the proton RF amplitude $\nu_1 = \omega_1/2\pi$ and the chemical shift difference between the coupled carbons, given by $\Delta^{cs}/2\pi$, at three different MAS frequencies. Several recoupling conditions are observed in the figure. Most efficient recoupling is achieved when $\Delta^{cs}/2\pi = 0$ or at the R^2 condition when $\Delta^{cs} = \omega_r$ (this is seen clearly in Fig. 2a, at $\Delta^{cs}/2\pi = 10$ kHz). The rest of the recoupling regions are attributed to the matching conditions given by Eq. (19). These conditions are plotted in white lines for the different n and n' values. As expected, significant recoupling occurs when the R^3 conditions are met (with either $n' = 1$ or 2). At these conditions the heteronuclear interactions have the largest effect and can cause a matching of the chemical shift difference for different crystallite orientations which makes the condition broad and not very sensitive to exact matching. Also for combinations of parameters away from R^3 there is significant recoupling, these regions are more local (and are linearly dependent on the RF amplitude) and can be derived using the van Vleck transformation (following route (a) as described above). This can be appreciated especially in the $\nu_r = 15$, 20 kHz plots, where $\Delta_{n',j}^{HC}$ is small compared to $(\omega_1 - n'\omega_r)$. They have been identified by Takegoshi et al. [16] using secular average Hamiltonian approach and were dabbed resonance interference recoupling (RIR) (for off rotary resonant cases).

The fact that at the R^3 regions the heteronuclear couplings are most efficiently recoupled makes them preferable for RAD/DARR recoupling in strongly coupled heteronuclear systems. In a sample with many carbon pairs the chemical shift difference commonly varies between $0 - 140$ ppm (or $0 - 14$ kHz at a 9.4 T magnet) thus the R^3 regions are more suitable for efficient recoupling in this range. As will be demonstrated, in the presence of proton homonuclear couplings this robustness is increased.

2.1.3. Proton homonuclear interactions

We will now consider the effect of additional protons coupled to the carbon pair. The homonuclear interactions between the protons can be added to the Floquet Hamiltonians (in the tilted frame) $\mathscr{H}_F^2$ and $\mathscr{H}_F^3$ in Eq. (11) as

$$\mathscr{H}_n^{HH} = \sum_{j,k} \omega_n^{jk} \left(\sqrt{\frac{3}{8}}(H_{2,jk}^{(2)} + H_{-2,jk}^{(2)}) - \frac{1}{2}H_{0,jk}^{(2)}\right) \tag{24}$$

where $\omega_n^{jk} = \sqrt{6}\omega_{jk} G_n^{jk}, \omega_{jk}$ are the dipolar couplings between protons j and k and G_n^{jk} are orientation dependent coefficients relating the dipolar vector to the lab frame [29]. The $H_{m,jk}^{(l)}$ are the spin irre-

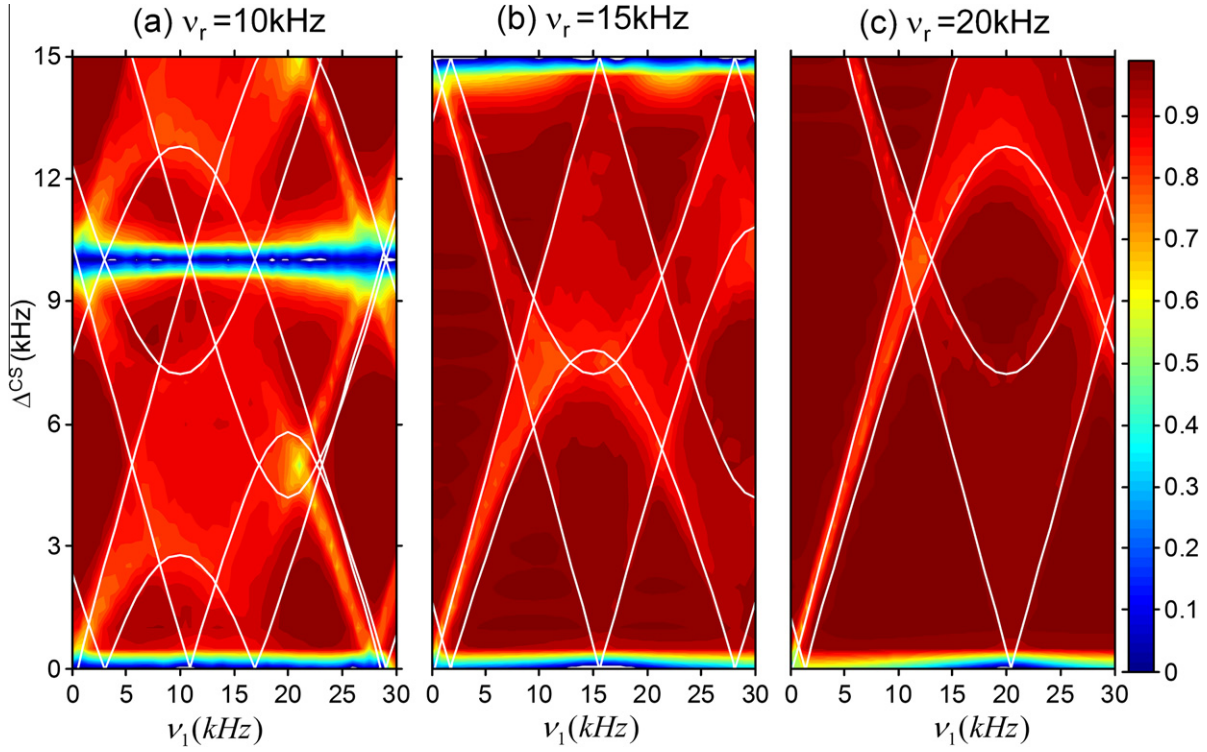

Fig. 2. The simulated signal intensity defined as $\langle C_z^{2-3}\rangle$ (15 *ms*) for a system of two carbons (with 2 kHz dipolar coupling) and a single proton (23 and 3 kHz heteronuclear couplings) averaged over a set of 1154 $\{\alpha,\beta,\gamma\}$ angles at 400 MHz ^{1}H Larmor frequency. The signal was calculated as a function of the isotropic chemical shift difference between the carbons and the RF amplitude of the protons at MAS frequency of 10 kHz (a), 15 kHz (b) and 20 kHz (c). Color bar represents the signal intensity with $\langle C_z^{2-3}\rangle(0) = 1$ and maximal recoupling with $\langle C_z^{2-3}\rangle = -1$. The solid white lines plotted on top are a result of an exact diagonalization, specifying conditions of efficient recoupling following Eq. (19) with dipolar couplings corresponding to a single crystal orientation.

ducible tensor operators. Due to its MAS time dependence the homonuclear *HH* interaction appears as off diagonal Floquet elements, along with the heteronuclear interaction. When the R^3 condition is approached, almost degenerate states $|2,\nu,\pi\rangle$ and $|2,\nu+n,\pi'\rangle$ with $\pi \neq \pi'$ (and similarly for the $|3\rangle$ subspace) can be connected by significant heteronuclear elements but not by homonuclear ones. Thus we can apply the same 'local' diagonalization as in Eq. (16):

$$\widetilde{\mathscr{H}}_F^{2-3} \simeq (D_F^{2-3})^{-1}\mathscr{H}_F^{2-3}(D_F^{2-3}) \tag{25}$$

D_F^{2-3} is again only a function of $\Delta_{n',j}^{CH}, \omega_1$ and $n'\omega_r$. However, unlike the simple case of a single proton, we have to take into account the contribution of the additional off diagonal elements originating from the homonuclear couplings and consider their contribution to the recoupling process. These can be evaluated by calculating $(D_F^2)^{-1}\mathscr{H}_n^{HH}F_nD_F^2$ and $(D_F^3)^{-1}\mathscr{H}_n^{HH}F_nD_F^3$, and it is reasonable to assume that mainly the resulting diagonal contributions given by $\widetilde{\mathscr{H}}_0^{HH,2}$ and $\widetilde{\mathscr{H}}_0^{HH,3}$ are significant. After this transformation $\widetilde{\mathscr{H}}_0^{HH,2}$ and $\widetilde{\mathscr{H}}_0^{HH,3}$ contribute differently (and anisotropically) to the diagonal elements and the recoupling condition of the *CC* interaction must be slightly modified and becomes a set of conditions:

$$\sqrt{\left|\frac{\Delta_{n',j}^{HC}}{2}\right|^2 + (\omega_1 - n'\omega_r)^2} + \tilde{\Delta}_{n'}^{jk} + n\omega_r = \Delta^{cs} \tag{26}$$

where $\tilde{\Delta}_{n'}^{jk} = \tilde{\omega}_n^{jk,2} - \tilde{\omega}_n^{jk,3}$, and $\tilde{\omega}_n^{jk}$ is calculated by applying the diagonalization matrices on the homonuclear interaction and extracting their diagonal contributions for the energies of states $|2,\nu,\pi\rangle$ and $|3,\nu+n,\pi'\rangle$ with $\pi \neq \pi'$. When one of the conditions in Eq. (26) is met, carbon pair recoupling via the *CC* interaction can occur. Thus we can expect that the homonuclear couplings between the protons will make the recoupling condition less sensitive to the RF amplitude and the chemical shift difference between the carbons. When a certain crystallite orientation does not match the condition in Eq. (19) it can still satisfy the condition in Eq. (26) assisted by the presence of the proton homonuclear couplings.

To demonstrate the effect of the proton homonuclear interaction we have performed similar simulations, as in Fig. 2, but only at the first R^3 condition with $\omega_1/2\pi = \omega_r/2\pi = 10$ kHz. The spin system used is composed of two carbons coupled to three protons and the result is plotted in Fig. 3a. The black line was calculated without the proton homonuclear couplings and the dotted gray line with them. It can be seen that the homonuclear couplings improve the polarization transfer process by allowing more crystallite orientations to match the recoupling condition in Eq. (26). Fairly constant recoupling efficiency is obtained, irrespective of the chemical shift difference between the carbons, except at the occurrence of the R^2 condition when $\Delta^{CS}/2\pi = 10$ kHz which is much more efficient.

2.1.4. Chemical shift anisotropy

The chemical shift anisotropy of the carbons can be added to the Floquet Hamiltonian as

$$\mathscr{H}_n^{CSA} = \Sigma_n^{csa}C_z^{1-4} + \Delta_n^{csa}C_z^{2-3}, \tag{27}$$

where $\Sigma_n^{csa} = \sigma_a g_n^a + \sigma_b g_n^b$ and $\Delta_n^{csa} = \sigma_a g_n^a - \sigma_b g_n^b$, σ is the chemical shift anisotropy and the g_n are the orientation dependent coefficients of the interaction [29]. As other anisotropic interactions, the CSA is also off diagonal in the Floquet representation, however, since it commutes with the isotropic chemical shift difference term of the carbon pair it can not affect the recoupling process significantly. It can only contribute via a first order mechanism, by forming a cross term with the *CC* interaction. This cross term can lead to recoupling when degeneracies are formed between the $|2\rangle$ and $|3\rangle$

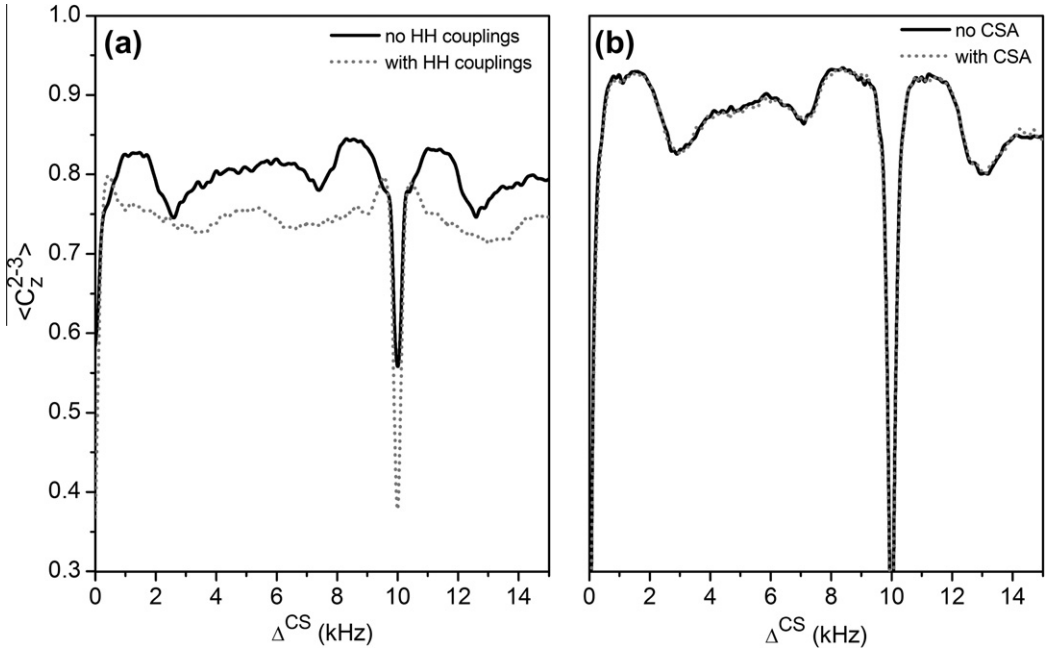

Fig. 3. The simulated signal, $\langle C_z^{2-3}\rangle(15\text{ ms})$, at 10 kHz MAS frequency and RF amplitude. The system used in (a) consisted of two carbons (2 kHz coupling) and three protons (heteronuclear couplings vary between 3 − 24 kHz) without homonuclear couplings (solid black) and with couplings in the range 8 − 24 kHz (in dotted gray). The system in (b) was identical to that in Fig. 2 and the signal was calculated without the carbons CSA (solid black) and with CSA (dotted gray) of 2 and 10.3 kHz at a 400 MHz ^{1}H Larmor frequency.

subspaces. However, we can expect that its influence is negligible relative to the *CC* interaction itself. An example of the effect of the CSA on the recoupling process is shown in Fig. 3b, where we have performed the simulations on a carbon pair system, coupled to a single proton at the condition of $\omega_1/2\pi = \omega_r/2\pi = 10$ kHz. Comparing the simulations performed without (in solid black) and with (in dotted gray) the carbons CSA interaction it is evident that no significant change in the recoupling efficiency is observed.

2.2. RF assisted recoupling through surrounding spin 1 nuclei

For the case of a carbon pair coupled to deuterium, with spin $I = 1$, the recoupling conditions must be re-examined by taking the quadrupole interaction into account. The deuterium quadrupole frequency is of the order of 100 kHz (for α and β sites in amino acids, for example) and it is thus the most significant interaction in the Hamiltonian of the system. Following the discussion above (Eq. (11)) we can again restrict ourselves to the $|2\rangle - |3\rangle$ subspace described in the case of a carbon pair coupled to a single deuterium nuclei by the Floquet Hamiltonian:

$$\mathscr{H}_F^{2-3} = \left(\mathscr{H}_0^{CS} + \mathscr{H}_0^{RF}\right)F_0 + \sum_n \left(\mathscr{H}_n^{CC} + \mathscr{H}_n^{DC} + \mathscr{H}_n^{Q}\right)F_n + \omega_r N \qquad (28)$$

$$\mathscr{H}_0^{CS} = \Delta^{cs} C_z^{2-3} \qquad (29)$$

$$\mathscr{H}_0^{RF} = \omega_1 D_x \qquad (30)$$

$$\mathscr{H}_n^{CC} = -\omega_{n,ab}^{CC} C_x^{2-3} \qquad (31)$$

$$\mathscr{H}_n^{DC} = \Delta_{n,j}^{DC} D_{z,j} C_z^{2-3} \qquad (32)$$

$$\mathscr{H}_n^{Q} = \omega_n^Q (3D_z^2 - D(D+1)) \qquad (33)$$

where $\omega_n^Q = \omega_Q g_n^Q/3$ and $\omega_Q/3 = eQeq/4\hbar$ is the quadrupole frequency with eQ the magnitude of the nuclear quadrupole moment and eq is the electric field gradient at the nucleus in the direction of the magnetic field [34]. The g_n^Q are coefficients relating the quadrupole principle axis system with the laboratory frame. Since $\mathscr{H}_n^Q$ is off diagonal and much larger than ω_r we cannot neglect its contributions as we did in the case of other smaller interactions. An exact diagonalization is required (described as route (c)) since we can not even apply the same approximation we have used in the case of the proton homonuclear dipolar couplings. For the diagonalization all the interactions involving the deuterium nucleus, namely $\mathscr{H}_0^{RF}$, $\mathscr{H}_n^{DC}$ and $\mathscr{H}_n^Q$, are taken into account. After performing the diagonalization we can identify the recoupling conditions leading to magnetization transfer between the carbon pair.

To demonstrate the effect of the quadrupole interaction on the recoupling process we have performed numerical simulations of a three spins system – two carbon nuclei and a single deuterium nucleus. As before, the observable $\langle C_z^{2-3}\rangle(\tau_{mix})$ was calculated as a function of the deuterium RF amplitude and chemical shift difference between the two carbons. The result is shown in Fig. 4a–c for $\chi = e^2Qq/\hbar$ values varying between 0 and 120 kHz. Without the presence of the quadrupole coupling (Fig. 4a) several lines of efficient recoupling are observed (in addition to the R^2 condition). The positions of these lines, in terms of the dependence on the chemical shift difference and the RF amplitude, are given by $\Delta^{CS} = m\nu_1 + n\omega_r$, with mainly $m = \pm 1$ and $|n| \leqslant 4$. Weaker lines appear at $m = \pm 2$ and $|n| = 1, 2$. Such dependence is typical for the formation of accidental degeneracies in the Floquet Hamiltonian. To understand this result we realize that for $\mathscr{H}_n^Q = 0$ all the off diagonal interactions in the Floquet Hamiltonian are very small compared to the diagonal elements ($|\Delta_{n,j}^{DC}| \ll |n\omega_r|$), thus van Vleck transformation can be applied to block diagonalize the Hamiltonian (route (b-i) above). The transformation removes the off diagonal elements and results in new, smaller, cross terms between the *CC* and *DC* interactions of the form

$$\widetilde{\mathscr{H}}_n^{CC-DC} = -\sum_{n'=\pm1,\pm2,j} \frac{\omega_{n-n',ab}^{CC}\Delta_{n',j}^{DC}}{n'\omega_r} D_{x,j} C_y^{2-3} \qquad (34)$$

with $-4 \leqslant n \leqslant 4$ and defined in a frame tilted in the direction of the RF irradiation (notice that this case, with no quadrupole interaction, is analog to systems with weak heteronuclear couplings between the carbons and spin 1/2, which can also be described by

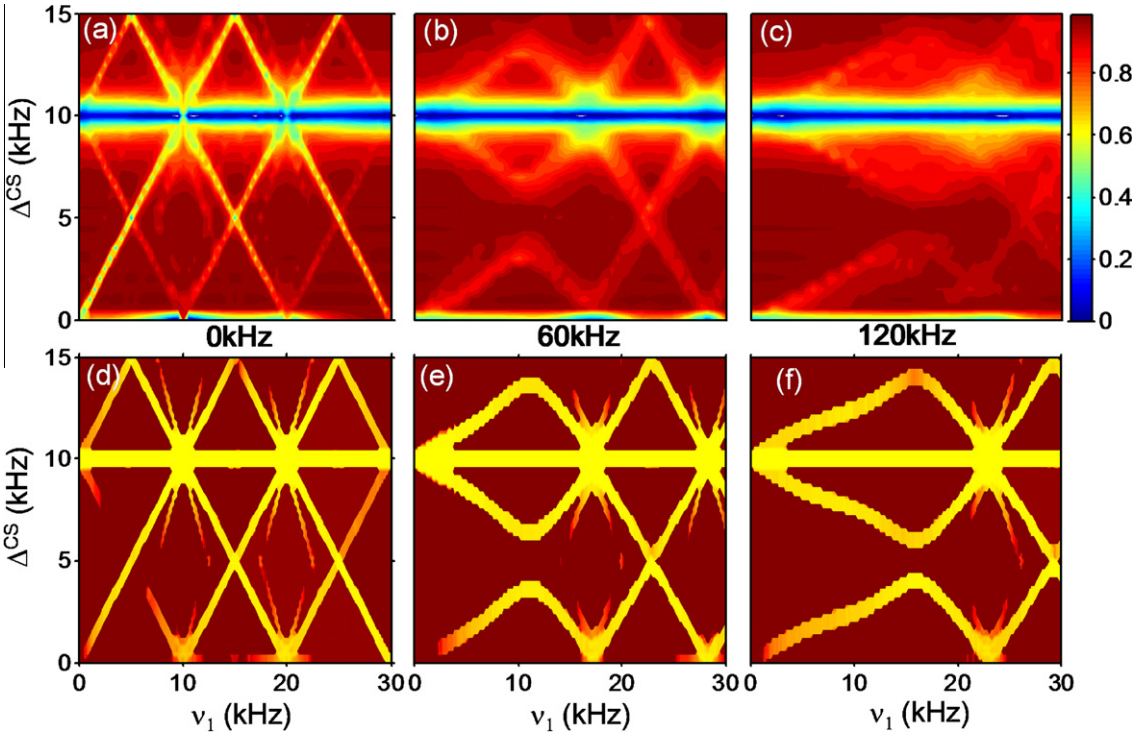

Fig. 4. The simulated signal, $\langle C_z^{2-3}\rangle$(15 ms), at 10 kHz MAS of the system described in Fig. 2 with deuterium nucleus instead of a proton. The quadrupole coupling was $\chi = 0$ in (a), 60 kHz in (b) and 120 kHz in (c). The signal was calculated as a function of the chemical shift difference between the carbons and ν_1^D. In plots d–f the conditions for recoupling were calculated by exact diagonalization (the procedure is described in the text).

Eq. (34)). Since these terms are off diagonal (in the diagonal or non diagonal Floquet blocks) they can only lead to recoupling if they connect degenerate diagonal states, when an accidental degeneracy is formed:

$$\Delta^{CS} = m\nu_1 + n\omega_r \tag{35}$$

$|m| = 1, 2$ and $-4 \leqslant n \leqslant 4$ (double quantum transitions with $|m| = 2$ are also expected through higher order terms formed at the accidental degeneracy). These recoupling conditions are indeed observed in Fig. 4a and we can conclude that when the quadrupole Hamiltonian is zero, or very small, they describe the recoupling mechanism. As the quadrupole coupling becomes larger (relative to ω_1 and ω_r) this simple description is no longer valid. This can be seen in Fig. 4b and c, where it is clear that with large (and realistic) coupling constants the recoupling conditions are not as well defined as in Fig. 4a, especially for low values of ω_1. In this case we separate the Hamiltonian into two parts-

$$\mathscr{H}_F^{2-3} = (\mathscr{H}_0^{RF}F_0 + \mathscr{H}_n^{DC}F_n + \mathscr{H}_n^{Q}F_n + \omega_r N) + (\mathscr{H}_0^{CS}F_0 + \mathscr{H}_n^{CC}F_n) \tag{36}$$

and diagonalize the first part by a diagonalization matrix D_F^{2-3} resulting in

$$\widetilde{\mathscr{H}}_F^{2-3} = \sum_j \omega_{eff} D_{zj} F_0 + (\mathscr{H}_0^{CS}F_0 + \left(D_F^{2-3}\right)^{-1}\mathscr{H}_n^{CC}F_n D_F^{2-3}) + \omega_r N \tag{37}$$

After the diagonalization of the diagonal blocks of $\mathscr{H}_F^2$ and $\mathscr{H}_F^3$ the Floquet states become $|2, v, \tilde{\pi}>$ and $|3, v, \tilde{\pi}>$, where $\tilde{\pi}$ are the deuterium spin states, which are a linear combination of the original π states (with $\pi = |-1>, |0>, |1>$). The exact form of these $\tilde{\pi}$ states depends on the details of the diagonalization and the reordering of the Fourier state. Following the discussion in the former section recoupling will occur when

$$< 2, v, \tilde{\pi}|\widetilde{\mathscr{H}}_F^{2-3}|2, v, \tilde{\pi}> = < 3, v+n, \tilde{\pi}'|\widetilde{\mathscr{H}}_F^{2-3}|3, v+n, \tilde{\pi}'>, \tag{38}$$

with $\tilde{\pi} \neq \tilde{\pi}'$ which result in the generalized RAD/DARR conditions for spin $I = 1$:

$$\Delta^{CS} = \omega_{eff} + n\omega_r \tag{39}$$

When these conditions are met, the carbon pair will be recoupled only if

$$< 2, v, \tilde{\pi}|(D_F^{2-3})^{-1}\mathscr{H}_{n'}^{CC}F_{n'}D_F^{2-3}|3, v+n, \tilde{\pi}'> \neq 0 \tag{40}$$

As in the former section, we can only expect a non zero off diagonal *CC* element connecting different deuterium $|\tilde{\pi}>$ states, when the heteronuclear interaction *DC* contributes finite values to the elements of $\widetilde{\mathscr{H}}_F^2$ and $\widetilde{\mathscr{H}}_F^3$ as well as to the diagonalization matrices. Since we perform an exact diagonalization (there is no trivial analytical expression for D_F^{2-3},) this approach is valid for the entire range of ω_1 and ω_Q used in the simulations. We do, however, expect that for small ω_Q or large ω_1 values this approach will converge to the approximate solution obtained with the van Vleck transformation. Notice also that due to the very large quadrupole off diagonal elements the values of ω_{eff} can deviate strongly from ω_1 causing a spread of recoupling conditions at many RF and chemical shift values in a powder sample. Thus, only in few crystallite orientations the carbon pair is recoupled for each combination of ω_1 and Δ^{CS} and overall the recoupling efficiency is not high.

In Fig. 4d–f the results of the exact diagonalization are presented for the system used in the simulations (choosing the geometric coefficients of all interactions as ~0.25 which correspond to a certain single crystal orientation) and limiting the Fourier states to $-25 \leqslant v \leqslant 25$. In order to evaluate the extent of recoupling in these figures we extracted the values of the off diagonal elements in Eq. (40) for values satisfying $|\Delta^{CS} - (\omega_{eff} + n\omega_r)| \leqslant$ 0.5 kHz (resulting in a certain width for the recoupling condition). Examining the form of the recoupled patterns we see that they

reproduce very nicely the results from our simulations for the whole range of interactions. With no quadrupole coupling (or in the range of large RF amplitudes) we get a linear dependence on ν_1 (following approximately Eq. (35)). As the interaction is increased exact diagonalization becomes inevitable. The results from the simulations were obtained using powder averaging. This leads to the smearing of the recoupling conditions, which is not observed in the calculation performed for a single crystal orientation.

In the case of deuterated systems we expect the influence of the homonuclear deuterium couplings to be very small and insignificant for the recoupling process.

2.3. Double nucleus enhanced recoupling

Finally we would like to consider the carbon homonuclear recoupling scheme which involves two RF frequencies; irradiating both proton $I = 1/2$ and deuterium $I = 1$ spins simultaneously. This scheme is useful in partially deuterated systems, where the majority of the protons have been replaced with deuterons. Experimentally it was found that this double irradiation, dubbed DONER, results in improved recoupling when both RF amplitudes equal the MAS frequency [26]. This experiment can be applied to (partially) deuterated proteins, where the backbone and side-chains are fully labeled with ^2H and the exchangeable proton sites, such as the amide and hydroxyl groups, are back exchanged to protons to some extent. Thus deuterons are directly attached to the carbons (as in the case we have previously considered) and the protons are further away. As a result the heteronuclear couplings *DC* and *HC* are comparable and the homonuclear *HH* couplings are not as dominant as in the fully protonated systems.

The relevant part of the Floquet Hamiltonian in this case can be approximated as follows

$$\mathscr{H}_F^{2-3} = (\mathscr{H}_0^{CS} + \mathscr{H}_0^{RF})F_0 + \sum_n (\mathscr{H}_n^{CC} + \mathscr{H}_n^{HC} + \mathscr{H}_n^{Q} + \mathscr{H}_n^{DC} + \mathscr{H}_n^{HD})F_n + \omega_r N \quad (41)$$

$$\mathscr{H}_0^{RF} = \omega_1 D_x + \omega_1 H_z \quad (42)$$

$$\mathscr{H}_n^{HD} = \sum_{j,k} \omega_{n,jk}^{HD} H_{x,j} D_{z,k} \quad (43)$$

with $\omega_{n,jk}^{HD} = \omega_{jk} G_{n,jk}^{HD}$ and all other interactions are as defined above. Here we have neglected the proton and deuterium homonuclear couplings. All operators are again defined by a product between the |2> and |3> subspaces with all proton and deuterium states, as well as with the Fourier states.

The only difference between this Hamiltonian and the former two cases (in Eq. (11) and Eq. (28)) is the presence of the heteronuclear couplings between the protons and deuterons. However these interactions are small (about 1 kHz) and do not influence directly the carbon states. Thus, if at all, they can only affect the recoupling process via high order terms formed after a van Vleck transformation of the Hamiltonian. Therefore we expect that the improved recoupling observed during double nucleus irradiation is a result of the sum of the two independent processes – recoupling through the *CH* and *CD* interactions autonomously.

To examine this we performed simulations on a system of two carbons coupled directly to two deuterium nuclei (one on each carbon) and indirectly to two protons. The extent of carbon recoupling under RF irradiation on ^{1}H and/or ^{2}H nuclei was evaluated from the simulated signal $\langle C_z^{2-3}\rangle(\tau_{mix} = 15\text{ ms})$ and is plotted in Fig. 5. In Fig. 5a and b the separate recoupling processes are demonstrated, with RF on the protons (a) and on the deuterons (b). Since the *CH* interactions are relatively weak (a few kHz only) the recoupling conditions are localized and appear at the positions expected from the formation of accidental degeneracies as in Eq. (35), for both single and double quantum conditions. Since the localization of these degeneracies is independent of the anisotropic interactions they are very well defined. When the RF is applied only on the deuterons we observe the patterns discussed in the former section since with quadrupole interactions beyond 100 kHz recoupling becomes a complicated function of both $\mathscr{H}_n^Q$ and $\mathscr{H}_n^{DC}$. Simultaneous RF irradiation (with equal amplitudes) resulted in the recoupling patterns plotted in Fig. 5c and d, where we have left the *HD* interactions intact in (d) and scaled them to zero in (c). A comparison of the two plots reveals that the recoupling patterns are practically identical, thus the *HD* couplings are probably not very contributing to the recoupling process (at least in this small system). Comparing the plots with (a) and (b) it seems that no new recoupling

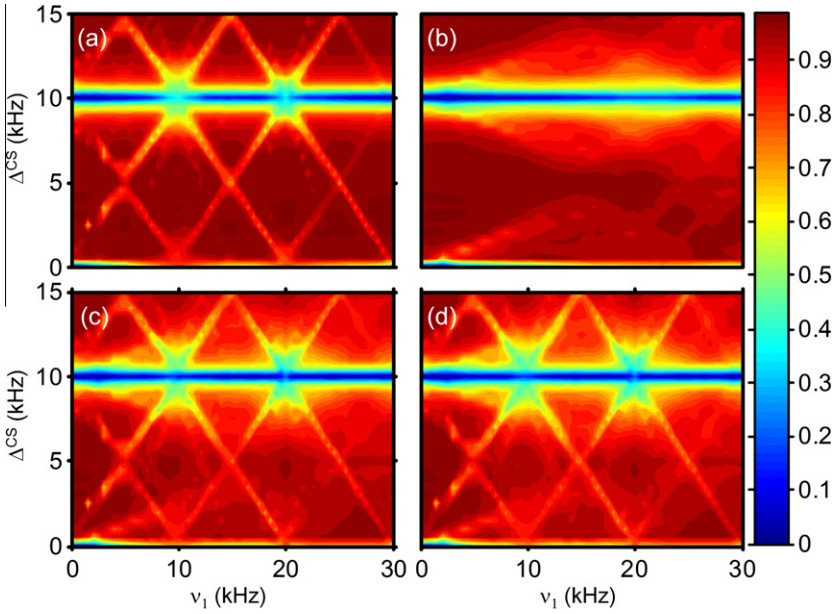

Fig. 5. The simulated signal, $\langle C_z^{2-3}\rangle$(15 ms), at 10 kHz MAS of the system of two carbons (2 kHz couplings) directly bonded to two deuterons (*CD* couplings between 0.5 − 3.4 kHz, χ = 120, 130 kHz and η = 0.2,0.8) and adjacent to two protons (with CH couplings 1.5 − 4 kHz). The signal was calculated as a function of the carbons chemical shift difference and ν_1^H with $\nu_1^D = 0$ in (a), ν_1^D with $\nu_1^H = 0$ in (b) and $\nu_1^D = \nu_1^H$ in (c) and (d). The *HD* couplings were scaled to zero in plots (a–c) and couplings in the range 0.5 − 1.5 kHz were added in (d).

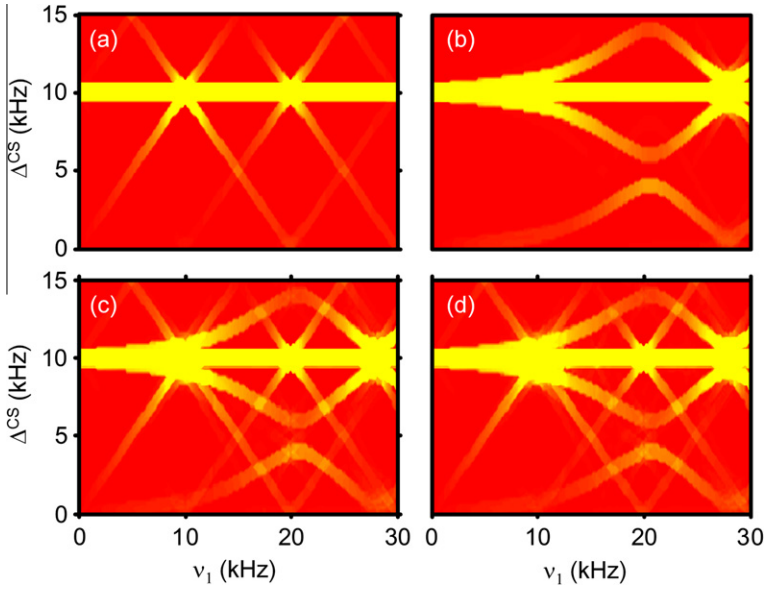

Fig. 6. Calculated recoupling conditions for a system of two carbons, a proton and a deuteron (χ = 120 kHz) following the procedure described in the text. The calculation was done as a function of the carbons chemical shift difference and ν_1^H with $\nu_1^D = 0$ in (a), ν_1^D with $\nu_1^H = 0$ in (b) and $\nu_1^D = \nu_1^H$ in (c) and (d). The *HD* couplings were scaled to zero in plots (a–c) and added in (d).

conditions were formed and that the two recoupling processes contributed simultaneously (and independently).

To further substantiate these results we have performed an exact diagonalization of the Hamiltonian describing a system of four spins – two carbon nuclei, one proton and one deuterium nucleus. The couplings chosen are of the order of the couplings used in the simulations. We have repeated the procedure described above for exact diagonalization of the Floquet Hamiltonian (for a slightly bigger system) and evaluated the recoupling extent by extracting the non zero elements as in Eq. (40) when the condition in Eq. (39) is met with a threshold of 0.5 kHz. The results of this calculation are shown in Fig. 6a–d. The cases of single RF irradiation on the proton and on the deuterium are shown in plots (a) and (b) respectively. As expected, for the small *CH* couplings all recoupling position (i.e. combinations of ω_1 and Δ^{CS}) follow Eq. (35) with ν_1 as the proton RF irradiation in this case. The deuterium case in Fig. 6b is very similar to the recoupling process discussed before, in Fig. 4c, and it leads to recoupling at positions dependent on all deuterium interactions. The combined effect of the two RF irradiations is shown in Fig. 6c and d with the *HD* couplings set equal to zero and to 1.5 kHz, respectively. From this exact calculation it can be appreciated that almost no new recoupling conditions are formed. The *HD* couplings lead only to very shallow new conditions in which the recoupled *CC* interaction is relatively small.

Thus we can conclude that in the relatively small systems considered here the DONER effect is a combination of the two separate generalized RAD/DARR processes of the ^{1}H and ^{2}H nuclei. To further support our theoretical observations experiments were performed on a partially deuterated model compound. In addition initial results are presented comparing these recoupling schemes on a perdeuterated protein.

3. Experiments

To demonstrate the effect of the recoupling schemes described above we have performed experiments on a partially deuterated model compound. The model compound studied was [U-^{13}C2, 2,2-D2,^{15}N]-glycine purchased from Cambridge Isotope Laboratories, Inc. and used without further purification. A powder of the compound was packed into a Bruker 4 mm zirconia rotor and centered between two Teflon spacers. Experiments were performed on a Bruker DSX 300 MHz and AvanceIII 500 MHz spectrometers with 4 mm triple resonance probes tuned to ^{1}H–^{13}C–^{2}H frequencies. RF amplitudes were calibrated by nutation experiments performed on adamantane and [U-D]-hexamethylbenzene for ^{1}H and ^{2}H irradiations respectively.

The pulse sequences used for recoupling are shown in Fig. 7a–d. On the ^{13}C channel the sequence is composed of a preparation period followed by a mixing time and detection. The ^{13}C RF offset is set exactly between the carbonyl, C_{CO}, and aliphatic, C_α, sites (separated by 133 ppm) and their magnetization components are allowed to evolve for a duration $\tau = 1/(2\Delta)$, where Δ is the chemical shift difference in Hz (equal to $\Delta^{CS}/2\pi$). When the two sites magnetization vectors are 180° out of phase they are aligned along the z direction with an additional $\pi/2$ pulse. They are recoupled during τ_{mix} either passively (with no RF irradiation, so called PDSD mixing) as in Fig. 7a and b, or by RF irradiation on the ^{1}H (Fig. 7c), ^{2}H (Fig. 7d) channels or both (Fig. 7e). The signal is then detected during ^{1}H cw decoupling with a single scan. The relaxation delays used in the experiments were set equal to roughly twice and four times the longitudinal relaxation times in the 300 and 500 MHz spectrometers, respectively. The MAS frequency was kept at 7 kHz in all experiments. The intensity of the signal acquired with the various recoupling schemes is given by $S(t) = \{C_{z,CO}(\tau_{mix}) - C_{z,\alpha}(\tau_{mix})\}/\{C_{z,CO}\ (0) - C_{z,\alpha}(0)\}$, where $C_{z,CO}$ and $C_{z,\alpha}$ are the z magnetization components of the carbonyl and alpha carbons respectively. The analysis was based on the lines intensity.

Experiments were compared to numerical simulations performed using the SPINEVOLUTION program [33]. The atomic coordinates for glycine were extracted from neutron diffraction data [35]. The dipolar couplings between the amine protons and surrounding nuclei were scaled by three to account for its dynamics. The deuterium nuclei quadrupole parameters were estimated as $\chi = e^2Qq/\hbar$ = 170 kHz and η = 0 (following Ref. [36]). Powder averaging was performed using 168 $\{\alpha,\beta\}$ pairs and 20 γ angles, increasing the number of orientations did not lead to different results. For the carbon nuclei, only the isotropic chemical shift was included in the simulations (the CSA effect was verified to be insignificant).

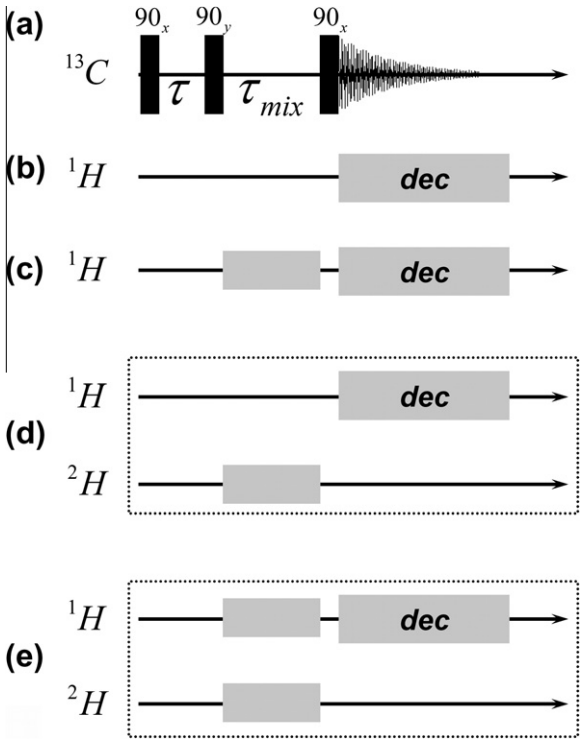

Fig. 7. The RF sequences used for carbon recoupling. The ^{13}C channel in (a) was used in all experiments, the ^1H sequence in (b) used for the PDSD experiment and in (c) for the RAD/DARR via ^1H recoupling. The ^1H and ^2H sequence in (d) was used for RAD/DARR via the deuterons and that in (e) was used for double nucleus enhanced recoupling.

Preliminary results comparing the recoupling mechanisms in ^{13}C–^{13}C correlation experiments where obtained by monitoring the cross peaks intensity acquired with various mixing schemes. These experiments were done on a 400 MHz Bruker spectrometer with a 3.2 mm Bruker triple resonance probe, at 10 kHz MAS frequency and temperature of 275 K. Full details on the pulse sequence can be found in ref. [26]. We have used a sample of perdeuterated alpha-spectrin SH3 domain [37,38] and the proton content of the sample (at the exchangeable sites) was tuned to 40% by re-crystallizing the protein in an appropriate H_2O/D_2O buffer. A detailed description of the sample preparation can be found in Ref. [37].

3.1. Results and discussion

The results of the 1D recoupling experiments on the model compound from the 300 and 500 MHz spectrometers are plotted in Fig. 8a–d. Let us first consider the signal obtained with recoupling by ^1H RF irradiation (sequence in Fig. 7a and c), these are plotted in black circles in Fig. 8a (300 MHz spectrometer) and c (500 MHz) for $\tau_{mix} = 10$ ms. On both spectrometers we observe similar behavior in which $S(t)$ is decreasing with the proton RF power and several distinct recoupling conditions are formed. Considering the chemical shift difference between the two sites in Hz we can expect that recoupling via the ^1H nuclei will be observed at $\nu_1^H = \Delta^{CS}/2\pi + n\nu_r$ (with $\nu_1^H = \omega_1^H/2\pi$ and $\nu_r = \omega_r/2\pi$). The recoupling conditions that are observed experimentally are for $n = 0, 1, 2, 3, 4$ (Fig. 8a) and for $n = -1, 0, 1, 2$ (Fig. 8c). These conditions correspond to Eq. (35), which can also be used to describe recoupling via ^1H nuclei when these are weakly coupled to the carbons. This is indeed the case in the measured sample, where the protons are not directly bound to the carbons resulting in relatively weak heteronuclear dipolar couplings which are additionally attenuated by the rotation of the amine group. As the RF amplitude decreases the experimental results can be roughly interpolated to the values observed with no RF irradiation (the sequence in Fig. 7a and b) for $\tau_{mix} = 10$ ms (marked with dashed black line).

To verify these effects the experimental data is compared to the simulated data (plotted in solid black lines). The simulation is in good agreement with the experimental results (at both fields) in terms of the positions of the recoupling conditions. However, comparing the experimental and simulation results, there is an additional effect which only appears in the former showing an overall decay in the signal as the RF power is decreased.

Next we consider the signal obtained after mixing with ^2H irradiation only (as in Fig. 7a and c). These results are plotted in black full circles in Fig. 8b and d for the 300 MHz and 500 MHz respectively. As expected, with large quadrupole couplings (of the order of 170 kHz), there are no well defined conditions for recoupling. For our model compound and the magnetic fields used we obtained maximal recoupling around $\nu_1^D = 23$ kHz and 20 kHz at 300 and 500 MHz respectively. The simulated data show a similar trend but the overall effect is a bit lower than that observed experimentally as was in the ^1H case.

The effect of both ^1H and ^2H irradiations simultaneously is also shown in Fig. 8b and d. The ^2H RF amplitude was varied while the proton irradiation was fixed at three values (corresponding to different recoupling efficiencies in Fig. 8a and c). The recoupling extent (manifested in a decrease in $S(t)$) after mixing with both RF irradiations is increased compared to the extent achieved with each of the irradiations separately. However, the profile as a function of the ^2H RF irradiation is independent of the proton RF amplitude and is identical to its profile with $\nu_1^H = 0$ kHz. From this we can infer that the two RF irradiations affect the signal independently and the overall effect is a contribution of the two. From these results we should not necessarily expect that the two mechanisms (recoupling via ^1H or ^2H irradiations) will operate constructively and it seems that there is some interference between them resulting in smaller effect than could be expected. The combination of the two RF fields does not lead to new recoupling conditions, as was already demonstrated in the theoretical section.

The fit we observe between the experimental results and the recoupling conditions derived theoretically and by simulations in Fig. 8a–d suggests that following the signal intensity after a fixed mixing period is a good measure for the recoupling extent. A more common observable is the build-up rate of cross peaks formed between interacting carbons or build-down rate of $S(t)$ as defined above. For a single crystal orientation rate measurements are indeed the only observable which can be used to compare recoupling processes which lead to $S(t)$ oscillating between 1 and −1. In a powder sample, however, this oscillation is attenuated or not observed and $S(t)$ reaches a plateau which is a good estimation for the robustness and extent of recoupling in the whole powder. To demonstrate this $S(t)$ was simulated as a function of the mixing time and either ν_1^H or ν_1^D. The values of $S(t_{\min})$, where $t_{\min}$ is the time when $S(t)$ reaches a minimal value, are plotted in Fig. 9a and b respectively for every RF amplitude. The values of $t_{\min}$ for several RF amplitudes are specified on the plot. These values are well correlated with the corresponding $S(t_{min})$ (i.e. when maximal recoupling is observed). Therefore efficient recoupling is observed at shorter mixing times and $S(\tau_{mix})$ is a good estimate of the recoupling process.

Next we consider the overall difference in the magnitude of the recoupling observed in the experimental results and the simulated ones. With both schemes, in Fig. 7c and d, we observe decreased signal intensity compared to that observed in the simulations. This difference does not arise from additional interactions present in the experimental system. This was verified by adding the chemical shift anisotropy of the ^{13}C nuclei and introducing additional

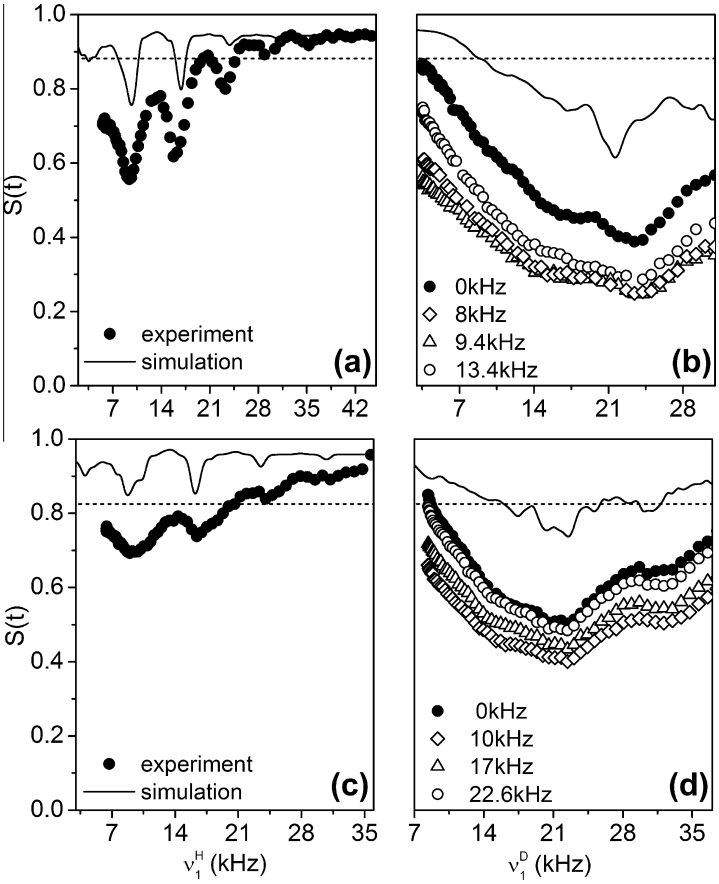

Fig. 8. Experimental results showing $S(t)$ on a 300 MHz spectrometer (top row) and 500 MHz (bottom). Full black circles correspond to experimental results obtained with a single RF irradiation, left column as function of ν_1^H with $\nu_1^D = 0$ and right column as a function of ν_1^D with $\nu_1^H = 0$ during τ_{mix}. Dashed lines represent the signal intensity acquired with no RF. Solid lines are the signal simulated with SPINEVOLUTION including all relevant nuclei from a single molecule of glycine. Data in circles, triangles and diamonds was acquired with simultaneous RF irradiations as a function of ν_1^D with fixed ν_1^H specified on the plot.

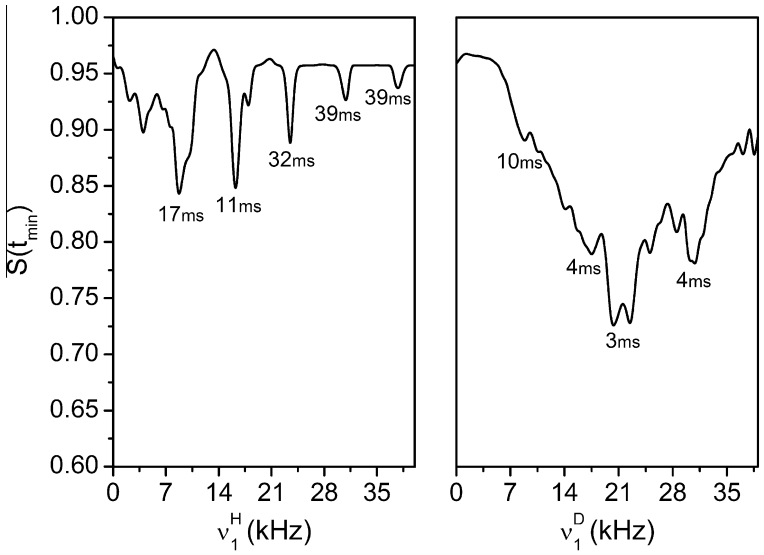

Fig. 9. Simulated signal of the glycine system at 500 MHz ^{1}H Larmor frequency. The values of $S(t_{min})$ are plotted as a function of ν_1^H (left) and ν_1^D (right). t_{min} is defined as the time the signal reaches a minimal value, corresponding to maximal recoupling. Representative values of t_{min} are specified on the plots.

protons/deuterons forming inter-molecular contacts, which did not lead to further decrease in the simulated signal. To study the source of this discrepancy we measured the signal on the 500 MHz spectrometer as a function of the mixing time, τ_{mix}, with a fixed RF amplitude, on either the ^{1}H or ^{2}H channels. The results are plotted in black dots in Fig. 10a and b. The simulated curves for the two cases are plotted in solid black lines and show a significant deviation from the experimental results. In order to fit our

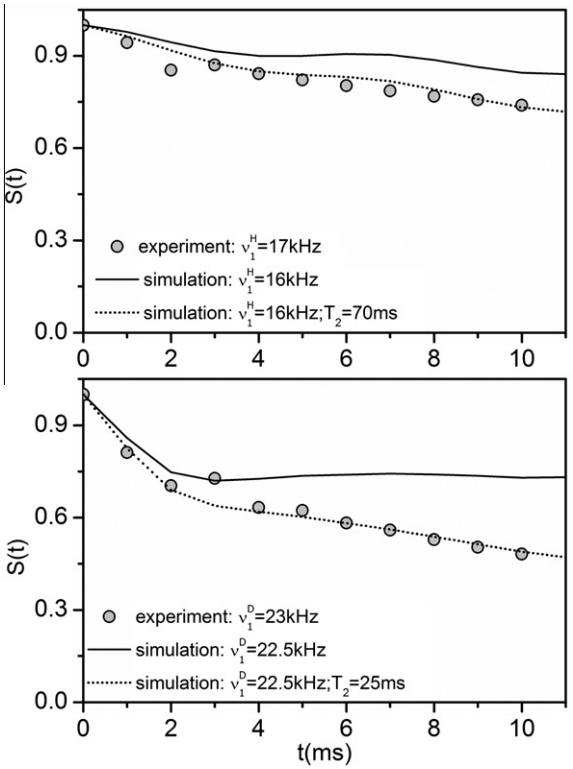

Fig. 10. Experimental results (gray circles) of $S(t)$ as a function of the mixing time on the 500 MHz spectrometer at 7 kHz MAS. $\nu_1^H = 17$ kHz (top) and $\nu_1^D = 23$ kHz (bottom). The simulated curves for similar conditions are plotted in solid black lines and after multiplication with a decaying exponential function in dotted lines.

simulations to the experimental results the simulated data was multiplied by a decaying exponent with a decay coefficient of 70 ms for the ^{1}H irradiation (Fig. 10a) and 25 ms for the ^{2}H irradiation (Fig. 10b). This processing resulted in the dashed lines which fit the experimental data well. We did not investigate further the source of this decay but it could be attributed to zero-quantum relaxation effects. Similar effects were observed by Levitt et al. in R^2 experiments where they were thoroughly studied and explained by the presence of zero-quantum transverse relaxation [39].

Finally we present initial results from a perdeuterated protein, a much larger system than our model compound. In this case we have compared the cross peaks intensities formed between $C_\alpha - C_\beta$ pairs in two residues of a perdeuterated alpha-spectrin SH3 domain. Cross-peak intensities are plotted as a function of the mixing time in a 2D ^{13}C–^{13}C correlation experiment in Fig. 11. Four mixing schemes are compared: PDSD (squares), ^{1}H RAD/DARR with $\nu_1^H = \nu_r = 10$ kHz (circles), ^{2}H RAD/DARR with $\nu_1^D = \nu_r = 10$ kHz (triangles) and DONER with $\nu_1^H = \nu_1^D = \nu_r = 10$ kHz (filled circles). For the two residues compared, T24 and K60, the cross peaks intensities are significantly different with the four mixing schemes with DONER leading to maximal recoupling. For K60, recoupling with DONER results in cross peaks which are more intense than the sum of those obtained with the two separate RF irradiations, while for T24 the DONER effect is lower than this sum. Thus we can expect that the contributions from the two RF fields would vary for different residues in the protein and most probably depend on the proton content around the recoupled carbons. These considerations and the optimization of the RF amplitudes for carbon mixing will be further discussed elsewhere [40].

4. Conclusions

Conditions for homonuclear recoupling via RF irradiation on strongly coupled proton systems were identified and discussed in the context of the RAD/DARR experiments. It was found that when the heteronuclear couplings are strong relative to the MAS frequency, recoupling occurs for a broad range of chemical shifts and is very efficient when the RF equals the MAS frequency. As the MAS frequency is increased recoupling becomes more localized and more selective to certain chemical shift values (as in Ref. [18]). This is similar to the mechanism in dilute proton systems, where the recoupling conditions occur at well defined RF amplitudes which depend on the MAS frequency and on the chemical shift difference. Recoupling via deuterons in deuterated systems was described for the first time using Floquet theory, taking into account a broad range of quadrupole couplings. It was shown that due to the quadrupole couplings there is only a weak dependence on the RF amplitude. Thus in these systems the R^3 condition is not necessarily the most efficient. With the combination of irradiating both protons and deuterons in a partially deuterated system almost no additional recoupling conditions are formed and the two processes operate independently, though the recoupling extent is not additive and there is some interference between the two mechanisms. Overall the combined effect achieved by simultaneous irradiation is bigger than in experiments with single RF irradiation and its extent depends on the details of the spin system. Further improvements with double irradiation can be expected by increasing the robustness of the proton assisted conditions, for example by additional modulation of the RF parameters. Experiments performed on a partially deuterated model compound suggest that for maximal recoupling the RF amplitude of the protons should

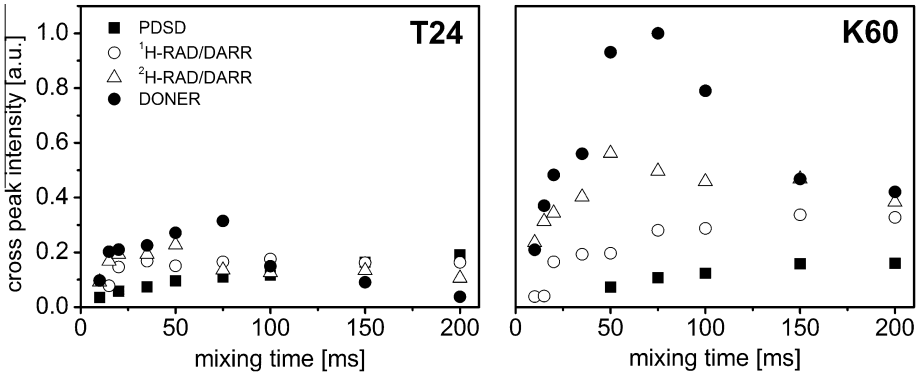

Fig. 11. Comparison of $C_\alpha - C_\beta$ cross peak intensities for the two selected residues (T24 and K60) in perdeuterated alpha spectrin SH3 domain extracted from several 2D ^{13}C–^{13}C correlation spectra. The MAS frequency was 10 kHz and the mixing schemes used were PDSD (squares), ^{1}H RAD/DARR with $\nu_1^H = 10$ kHz (circles), ^{2}H RAD/DARR with $\nu_1^D = 10$ kHz (triangles) and DONER with $\nu_1^H = \nu_1^D = 10$ kHz (full circles).

be optimized and that of the deuterons used at RF amplitudes exceeding the MAS frequency. Although our theoretical description did not take into account the effect of relaxation on the mixing of homonuclear pairs we could reproduce general trends in the dependence on the RF amplitudes and identify the significant recoupling conditions. These effects should be further investigated in perdeuterated proteins.

Acknowledgments

We acknowledge support from the Israel Science Foundation. We thank Prof. Asher Schmidt for letting us use the AvanceIII 500 MHz spectrometer. The research is made possible in part by the historic generosity of the Harold Perlman family. We acknowledge also the EU FP7 infrastructure project Bio-NMR (Grant No. 261863, HO).

References

[1] A. McDermott, Structure and dynamics of membrane proteins by magic angle spinning solid-state NMR, Annu. Rev. Biophys. 38 (2009) 385.
[2] H. Heise, Solid-state NMR spectroscopy of amyloid proteins, ChemBioChem 9 (2008) 179.
[3] D.P. Raleigh, M.H. Levitt, R.G. Griffin, Rotational resonance in solid state NMR, Chem. Phys. Lett. 146 (1988) 71.
[4] M.H. Levitt, D.P. Raleigh, F. Creuzet, R.G. Griffin, Theory and simulations of homonuclear spin pair systems in rotating solids, J. Chem. Phys. 92 (1990) 6347.
[5] R. Tycko, G. Dabbagh, Double-quantum filtering in magic-angle-spinning NMR spectroscopy: an approach to spectral simplification and molecular structure determination, Chem. Phys. Lett. 173 (1990) 461.
[6] R. Tycko, G. Dabbagh, Double-quantum filtering in magic-angle-spinning NMR spectroscopy: an approach to spectral simplification and molecular structure determination, J. Am. Chem. Soc. 113 (1991) 9444.
[7] A.E. Bennett, J.H. Ok, R.G. Griffin, S. Vega, Chemical shift correlation spectroscopy in rotating solids: radio frequency-driven dipolar recoupling and longitudinal exchange, J. Chem. Phys. 96 (1992) 8624.
[8] N.C. Nielsen, H. Bildsøe, H.J. Jakobsen, M.H. Levitt, Double-quantum homonuclear rotary resonance: efficient dipolar recovery in magic-angle spinning nuclear magnetic resonance, J. Chem. Phys. 101 (1984) 1805.
[9] M. Howhy, H.J. Jakobsen, M. Eden, M.H. Levitt, N.C. Nielsen, Broadband dipolar recoupling in the nuclear magnetic resonance of rotating solids: a compensated C7 pulse sequence, J. Chem. Phys. 108 (1998) 2686.
[10] Hohwy, C.M. Rienstra, C.P. Jaroniec, R.G. Griffin, Fivefold symmetric homonuclear dipolar recoupling in rotating solids: application to double quantum spectroscopy, J. Chem. Phys. 110 (1999) 7983.
[11] R. Tycko, Stochastic dipolar recoupling in nuclear magnetic resonance of solids, Phys. Rev. Lett. 99 (2007) 187601.
[12] V. Ladizhansky, Homonuclear dipolar recoupling techniques for structure determination in uniformly 13C-labeled proteins, Solid State Nucl. Magn. Reson. 36 (2009) 119.
[13] N. Bloembergen, On the interaction of nuclear spins in a crystalline lattice, Physica 15 (1949) 386–426.
[14] T.G. Oas, R.G. Griffin, M.H. Levitt, Rotary resonance recoupling of dipolar interactions in solid state nuclear magnetic resonance spectroscopy, J. Chem. Phys. 89 (1988) 692.
[15] K. Takegoshi, S. Nakamura, T. Terao, ^{13}C–^{1}H dipolar assisted rotational resonance in magic angle spinning NMR, Chem. Phys. Lett. 344 (2001) 631.
[16] K. Takegoshi, S. Nakamura, T. Terao, ^{13}C–^{1}H dipolar-driven ^{13}C–^{13}C recoupling without ^{13}C RF irradiation in nuclear magnetic resonance of rotating solids.
[17] C.R. Morcombe, V. Gaponenko, R.A. Byrd, K.W. Zilm, Diluting abundant spins by isotope edited radio frequency field assisted diffusion, J. Am. Chem. Soc. 126 (2004) 7196.
[18] I. Scholz, M. Huber, T. Manolikas, B.H. Meier, M. Ernst, MIRROR recoupling and its application to spin diffusion under fast magic-angle spinning, Chem. Phys. Lett. 460 (2008) 278.
[19] M. Weingarth, G. Bodenhausen, P. Tekely, Broadband carbon-13 correlation spectra of microcrystalline proteins in very high magnetic fields, J. Am. Chem. Soc. 131 (2009) 13937.
[20] G. De Paepe, J.R. Lewandowski, A. Loquet, A. Bockmann, R.G. Griffin, Proton assisted recoupling and protein structure determination, J. Chem. Phys. 129 (2008) 245101.
[21] I. Scholz, B.H. Meier, M. Ernst, NMR polarization transfer by second order resonant recoupling: RESORT, Chem. Phys. Lett. 485 (2010) 335.
[22] A.E. McDermott, F.J. Creuzet, A.C. Kolbert, R.G. Griffin, High-resolution magic-angle-spinning NMR spectra of protons in deuterated solids, J. Magn. Reson. 98 (1992) 408.
[23] L. Zheng, L.W. Fishbein, R.G. Griffin, J. Herzfeld, Two-dimensional solid-state proton NMR and proton exchange, J. Am. Chem. Soc. 115 (1993) 6254.
[24] C.R. Morcombe, E.K. Paulson, V. Gaponenko, R.A. Byrd, K.W. Zilm, ^{1}H–^{15}N correlation spectroscopy of nanocrystalline proteins, J. Biomol. NMR 31 (2005) 217.
[25] M. Hologne, V. Chevelkov, B. Reif, Deuterated peptides and proteins in MAS solid-state NMR, Prog. Nucl. Magn. Reson. Spectrosc. 48 (2006) 211.
[26] U. Akbey, H. Oschkinat, B.J. van Rossum, Double-nucleus enhanced recoupling for efficient ^{13}C MAS NMR correlation spectroscopy of perdeuterated proteins, J. Am. Chem. Soc. 131 (2009) 17054.
[27] K.Y. Huang, A.B. Siemer, A.E. Mcdermott, Homonuclear mixing sequences for perdeuterated proteins, J. Magn. Reson. 208 (2011) 122.
[28] I. Scholz, J.D. van Beek, M. Ernst, Operator based Floquet theory in solid state NMR, Solid State Nucl. Magn. Reson. 37 (2010) 39.
[29] A.E. Bennett, R.G. Griffin, V. Vega, Recouling of homo-heteronuclear dipolar interactions in rotating solids, NMR Basic Princ. Prog. 33 (1994) 1.
[30] M. Leskes, P.K. Madhu, S. Vega, Floquet theory in solid-state nuclear magnetic resonance, Prog. Nucl. Magn. Reson. 57 (2010) 345.
[31] S. Vega, Fictitious spin 1/2 operator formalism for multiple quantum NMR, J. Chem. Phys. 68 (1978) 5518.
[32] J.H. van Vleck, On U3c3-type doubling and electron spin in the spectra of diatomic molecules, Phys. Rev. 33 (1929) 467.
[33] M. Veshtort, R.G. Griffin, Spinevolution: a powerful tool for the simulation of solid and liquid state NMR experiments, J. Magn. Reson. 178 (2006) 248.
[34] K. Schmidt-Rohr, H.W. Spiess, Multidimensional solid-state NMR and polymers, Academic, London, 1994.
[35] M. Langan, S.A. Mason, D. Mylesc, B.P. Schoenborn, Structural characterization of crystals of a-glycine during anomalous electrical behaviour, Acta Crystallogr., Sect. B: Struct. Sci. 58 (2002) 728.
[36] C. Muller, W. Schajor, H. Zimmermann, U. Haeberlen, Deuteron chemical shift and EFG tensors in alpha-Glycine, J. Magn. Reson. 56 (1984) 235.
[37] U. Akbey, S. Lange, W.T. Franks, R. Linser, K. Rehbein, A. Diehl, B.J. van Rossum, B. Reif, H. Oschkinat, Optimum levels of exchangeable protons in perdeuterated proteins for proton detection in MAS solid-state NMR spectroscopy, J. Biomol. NMR 46 (2010) 67.
[38] V. Chevelkov, K. Rehbein, A. Diehl, B. Reif, Ultrahigh resolution in proton solid-state NMR spectroscopy at high levels of deuteration, Angew. Chem., Int. Ed. 45 (2006) 3878.
[39] M.H. Levitt, D.P. Raleigh, F. Creuzet, R.G. Griffin, Theory and simulations of homonuclear spin pair systems in rotating solids, J. Chem. Phys. 92 (1990) 6347.
[40] U. Akbey, H. Oschkinat, B.J. van Rossum, in preparation.